

# A Generic Pump-free Organ-on-a-Chip Platform for Assessment of Drug Bioavailability

Yaqiong Guo<sup>1</sup>, Yingying Xie<sup>1</sup>, and Jianhua Qin<sup>1</sup>

<sup>1</sup>Dalian Institute of Chemical Physics Department of Biotechnology

August 4, 2023

## Abstract

Organ-on-a-chip technology has shown great potential in disease modeling and drug evaluation. However, traditional organ-on-a-chip devices are mostly pump-dependent with low throughput, which makes it difficult to leverage their advantages. In this study, we have developed a generic, pump-free organ-on-a-chip platform consisting of a 32-unit chip and an adjustable rocker, facilitating high-throughput dynamic cell culture with straightforward operation. By utilizing the rocker to induce periodic fluid forces, we can achieve fluidic conditions similar to those obtained with traditional pump-based systems. Through constructing a gut-on-a-chip model, we observed remarkable enhancements in the expression of barrier-associated proteins and the spatial distribution of differentiated intestinal cells compared to static culture. Furthermore, RNA sequencing analysis unveiled enriched pathways associated with cell proliferation, lipid transport and drug metabolism, indicating the ability of the platform to mimic critical physiological processes. Additionally, we tested seven drugs which represent a range of high, medium, and low in vivo permeability using this model and found a strong correlation between their Papp values and human Fa, indicating reliable and predictive simulation outcomes for drug absorption. Our findings highlight the potential of this pump-free organ-on-a-chip platform as a valuable tool for advancing drug development and enabling personalized medicine.

## A Generic Pump-free Organ-on-a-Chip Platform for Assessment of Drug Bioavailability

Yaqiong Guo<sup>1\*</sup>, Yingying Xie<sup>1,5\*</sup>, Jianhua Qin<sup>1,2,3,4,5</sup>

<sup>1</sup>Division of Biotechnology, Dalian Institute of Chemical Physics, Chinese Academy of Sciences, Dalian, China

<sup>2</sup>Beijing Institute for Stem Cell and Regenerative Medicine, Chinese Academy of Sciences, Beijing, China.

<sup>3</sup>University of Science and Technology of China, Hefei, China

<sup>4</sup>Suzhou Institute for Advanced Research, University of Science and Technology of China, Suzhou, China

<sup>5</sup>University of Chinese Academy of Sciences, Beijing, China.

\* These authors equally contributed to this work.

Corresponding author: Jianhua Qin.

E-mail address: [jqin@dicp.ac.cn](mailto:jhqin@dicp.ac.cn)

**Key words** : organ-on-a-chip, in-vitro model, high-throughput, drug testing

**Abbreviations used in the paper:**

CCK-8: Cell counting kit-8 assay

Fa: fraction absorbed  
FBS: fetal bovine serum  
FITC: fluorescein isothiocyanate  
GO: gene ontology  
H&E: Hematoxylin and eosin  
HBSS: Hank's Balanced Salt Solution  
KEGG: Kyoto Encyclopedia of Genes and Genomes  
 $P_{app}$ : apparent permeability coefficient  
PBS: phosphate-buffered saline  
PC: polycarbonate  
PET: polyethylene terephthalate  
PFA: paraformaldehyde  
PS: penicillin/streptomycin  
RNA-Seq: RNA sequencing  
SEM: scanning electron microscopy  
TEER: transepithelial electrical resistance

### **Abstract:**

Organ-on-a-chip technology has shown great potential in disease modeling and drug evaluation. However, traditional organ-on-a-chip devices are mostly pump-dependent with low throughput, which makes it difficult to leverage their advantages. In this study, we have developed a generic, pump-free organ-on-a-chip platform consisting of a 32-unit chip and an adjustable rocker, facilitating high-throughput dynamic cell culture with straightforward operation. By utilizing the rocker to induce periodic fluid forces, we can achieve fluidic conditions similar to those obtained with traditional pump-based systems. Through constructing a gut-on-a-chip model, we observed remarkable enhancements in the expression of barrier-associated proteins and the spatial distribution of differentiated intestinal cells compared to static culture. Furthermore, RNA sequencing analysis unveiled enriched pathways associated with cell proliferation, lipid transport and drug metabolism, indicating the ability of the platform to mimic critical physiological processes. Additionally, we tested seven drugs which represent a range of high, medium, and low *in vivo* permeability using this model and found a strong correlation between their  $P_{app}$  values and human Fa, indicating reliable and predictive simulation outcomes for drug absorption. Our findings highlight the potential of this pump-free organ-on-a-chip platform as a valuable tool for advancing drug development and enabling personalized medicine.

### **Introduction**

In the recent decade, researchers have continuously developed many *in vitro* models, from 2D to 3D, and particularly, organ chips have evolved from conceptual to powerful tools that hold the potential to partially replace traditional *in vitro* models and animal models.<sup>[1-3]</sup> Nevertheless, the widespread adoption of organ chip systems currently faces certain challenges, including the reliance on labor-intensive external pumps and limited throughput.<sup>[4-6]</sup> In addition, although microfluidic systems reduce the use of cells and drugs, they also increase the difficulty of characterization and detection. For example, more precise manual operations or complex sensors are often required when measuring TEER, which can be challenging to achieve in small chips.<sup>[7, 8]</sup> Overcoming these challenges necessitates addressing both biological and engineering obstacles. This endeavor entails developing innovative microfluidic designs or platforms capable of precisely

controlling the flow of fluids, as well as establishing reproducible and physiologically relevant cell culture microenvironment.<sup>[9-11]</sup>

Currently, a variety of organ chips, such as intestine-on-a-chip,<sup>[12]</sup>liver-on-a-chip,<sup>[13]</sup>brain-on-a-chip,<sup>[14]</sup> have been developed. Of the various organ-on-chip devices, the intestine-on-a-chip are one of the most widely used models. A traditional intestine-on-a-chip is typically composed of two channels separated by a porous membrane lined with intestinal epithelial cells.<sup>[15-17]</sup> To replicate the dynamic in vivo microenvironment, the medium is commonly circulated through the channels using either syringes or peristaltic pumps. Intestine-on-a-chip systems allow for the analysis of drug absorption, toxicity, and efficacy, as well as the simulation of intricate host-microbe interactions.<sup>[18-21]</sup>

As we all know, the Caco-2 monolayer cultured on a transwell insert is widely recognized as one of the most commonly utilized models for studying human intestinal barrier absorption due to its simplicity and cost-effectiveness.<sup>[22]</sup> However, despite the widespread use of the transwell model in research, the cell culture process involved a prolonged time period, and the two-dimensional growth of cells in static culture does not entirely replicate the in vivo environment.<sup>[23, 24]</sup> Due to the effectiveness of organ chips in advancing the development of novel drugs and therapies, it offers a more physiologically relevant and reproducible alternative to traditional in vitro models.<sup>[25]</sup> On the other hand, existing chips used for drug evaluation often require high-precision instruments for detection due to low drug volume, which potentially increases the cost of application. Therefore, developing a high-throughput organ chip system that eliminates the need for complex pumps and valves has the potential to revolutionize drug discovery and toxicity testing.

In this study, we present a generic, pump-free and high-throughput 3D organ-on-a-chip platform that enables dynamic cell culture in vitro similar to traditional chip system. A rocker was utilized to generate periodic fluid force in our system which replaces the pump and intertwined pipelines. Using our platform, we established a gut-on-a-chip system that simulates human intestine. 3D stereoscopic structure and enhanced expression of intestinal barrier-associated proteins (ZO-1) was observed in our platform, which was deficient in static cultures. We also observed the spatial distribution of differentiated (Villin, MUC-2) and proliferative cells (Ki67) markers, suggesting that cell differentiation on the chip occurs similarly to that in vivo. RNA sequencing analysis demonstrated that cells showed significantly enriched pathways and up-regulated genes associated with drug metabolism function compared to those in static cultures. Based on these findings, we evaluated the drug bioavailability using our platform and achieved reliable and predictive simulation results, thus providing a promising tool for predicting the intestinal drug absorption of new drugs and a valuable asset for drug development and personalized medicine.

## Materials and Methods

### Device fabrication

The upper and lower layers of the chip were designed using SolidWorks software and sent to Shenzhen Future Factory for mold production and injection molding. After chip cleaning, the ultra-thin double-sided adhesive was precisely cut into the defined shape and then being used to securely encapsulate a polyethylene PET film between the upper and lower layers of the chip in a controlled dust-free environment. The PET film had a thickness of 10  $\mu\text{m}$  and a pore size of 2  $\mu\text{m}$ . To ensure the sterile conditions for cell culture, the assembled chips underwent overnight UV irradiation and additionally treated with a 5% PS solution for a minimum of 4 hours before being utilized. The specific chip size can be obtained in fig. S1.

### Cell culture

Caco-2 cells were cultured in high-glucose Dulbecco's modified Eagle's medium supplemented with 10% FBS and 1% PS. HT-29 cells were maintained in McCoy's 5A medium supplemented with 10% FBS and 1% PS. All cells were cultured in an incubator maintained at 37 with a 5% CO<sub>2</sub> atmosphere. All cell culture reagents are purchased from Gibco.

To seed the cells on the PET membrane, a ratio of 9:1 was used, resulting in a total cell count of approximately

50,000 cells. The cell-seeded chips were then placed on a rocker operating at 10 rpm and  $\pm 8^\circ$ , facilitating gentle fluid perturbation within the middle hole and ensuring regular fluid flow in the underlying channels. The culture medium was refreshed every two days to maintain cell viability and provide essential nutrients for growth. In terms of media supplementation, 150  $\mu\text{L}$  was introduced into the middle hole of the chip, while 600  $\mu\text{L}$  was added to the lower layer. This allocation aimed to maintain fluid level equilibrium between the middle hole and the two side holes, and ensuring adequate nutrient supply and waste removal throughout the experiment.

### **Finite element simulation**

Simulations were conducted using the "two-phase laminar flow" and "incompressible Navier-Stokes" application modes within the Comsol Multiphysics Finite Element Program (COMSOL 3.5, Comsol AB, Burlington) to visualize the flow characteristics along the centerline of the upper and lower surfaces of the membrane. The oscillatory motion was applied with the bottom center point as the axis, employing an angular displacement of  $\pm 8^\circ$  and a period of 6 seconds. The results revealed that the distribution of fluid shear stress on the membrane surface exhibited intermediate symmetry and temporal variation.

### **Live/Dead staining**

Following the protocol of the LIVE/DEAD® Viability/Cytotoxicity Assay Kit (Invitrogen, America), a working solution was prepared by combining 20  $\mu\text{L}$  of EthD-1 stock solution and 5  $\mu\text{L}$  of calcein AM stock solution in 10 mL of D-PBS (Meilunbio, China). This working solution was applied to cells that had undergone two washes with D-PBS. After a 30-minute incubation, fluorescence microscopy was employed to capture images.

### **CCK-8 assay**

On the sixth day of culture, a complete medium containing 10% CCK-8 (Meilunbio, China) was prepared. The cells were washed twice with PBS and then treated with the respective FITC-dextran solutions. After one and two hours of treatment, 100  $\mu\text{L}$  of medium from the lower layer was collected to measure the fluorescence intensity using a plate reader (Infinite® 200 PRO, Tecan, Switzerland).

### **Immunofluorescence imaging**

The PET membrane with cells was carefully excised, and washed with PBS twice. Subsequently, the cells were fixed with 4% PFA for 15 minutes. Permeabilization was achieved by treating the cells with 0.2% Triton X-100 for 7 minutes, followed by blocking with goat serum for 40 minutes at room temperature. The samples were then incubated overnight at 4  $^\circ\text{C}$  with a diluted antibody solution of ZO-1 (Abcam, ab221547, UK), MUC-2 (Abcam, ab11197, UK), Villin (Abcam, ab109516, UK) or Ki67 (Abcam, ab16667, UK), and subsequently with secondary antibodies at room temperature for 1 hour, protected from light. Hoechst (Meilunbio, China) staining was used to visualize the nuclei. For visualization of F-actin, samples were stained with phalloidin (Solarbio, China). Washing with PBS was performed three times. Confocal microscopy (FV-1000; Olympus, Tokyo, Japan) was utilized to capture images. Image processing was conducted using Image J.

### **H&E staining imaging**

The PET membrane with cells was cut off carefully, washed with PBS twice and fixed with 4% PFA for more than 24 hours and dehydrated in a graded series of alcohols in a dehydrator followed by being embedded in paraffin and sliced. Then, the paraffin-embedded sample was dewaxed in an environmentally friendly dewaxing solution, followed by dehydration in a series of alcohol solutions and a final water wash. The sections were stained with Hematoxylin for 3-5 minutes, rinsed with water, differentiated, rinsed again, and counterstained with Eosin for 5 minutes. Then the sections were dehydrated in a series of alcohol solutions and cleared with xylene, and mounted with neutral resin. Finally, the sections were viewed under a microscope, and images were taken for analysis. The cell nuclei appear blue, while the cytoplasm appears red.

### **SEM imaging**

To prepare a sample for SEM imaging, PET membrane with fixed cells were washed with PBS and then fixed with electron microscopy fixative. The sample was then washed with PBS for 3 times (15 min each) and post-fixed with OsO<sub>4</sub>. After being dehydrated with a series of ethanol concentrations (30%, 50%, 70%, 80%, 90%, 95% ethanol for 15 min, two changes of 100% ethanol for 15 min and isoamyl acetate for 15 min), the sample was dried with a critical point dryer, attached to metallic stubs, and coated with gold before being observed and imaged with a scanning electron microscope.

### **TEER measurement**

The TEER measurement was based on commercial EVOM3 instrument (World Precision Instruments, America) and a simple device compatible with our chip for measuring TEER was designed (**Fig. S2**). Four platinum wires were fixed on the PC cover after being cleaned several times with Piranha solution (A mixture of concentrated sulfuric acid and 30% hydrogen peroxide (3:1)), acetone, ethanol, and water, directly inserting into the solution as electrodes after sterilization by wiping with 70% ethanol. Washed the cell by PBS buffer once and the measurement was carried out in the PBS after the electrode was soaked in PBS for half an hour before use. The blank channel of the chip was measured in PBS before inoculating cells as blank control.

### **Permeability test**

FITC labeled dextran with molecular weights of 40 kDa and 4 kDa was prepared at a concentration of 1 mg/ml using complete medium. The cells were washed twice with PBS and then treated with the respective FITC-dextran solutions. After one hour and two hours of treatment, 100  $\mu$ L of medium from the lower layer was collected to measure the fluorescence intensity using a plate reader (Infinite® 200 PRO, Tecan, Switzerland).

### **RNA sequencing**

Total RNAs were extracted using TRIzol Reagent and DNA digestion was performed using DNase I. The quality of RNA samples was assessed by measuring the A260/A280 ratio using the Nanodrop™ One spectrophotometer (Thermo Fisher Scientific Inc). Furthermore, RNA integrity was confirmed by conducting 1.5% agarose gel electrophoresis. Finally, qualified RNA samples were quantified using the Qubit3.0 with the Qubit™ RNA Broad Range Assay kit (Life Technologies, Q10210). For stranded RNA sequencing library preparation, 2  $\mu$ g of total RNA was utilized. The KC-Digital™ Stranded mRNA Library Prep Kit for Illumina® (Catalog NO. DR08502, Wuhan Seqhealth Co., Ltd., China) was employed, following the manufacturer's instructions. This kit incorporates unique molecular identifiers consisting of 8 random bases to label the pre-amplified cDNA molecules. This approach helps to mitigate duplication bias during PCR and sequencing steps. Library products within the range of 200-500 bps were enriched, quantified, and subsequently sequenced on the DNBSEQ-T7 sequencer (MGI Tech Co., Ltd., China) using the PE150 model.

### **RNA-Seq data analysis**

The initial raw sequencing data underwent preprocessing steps. Trimmomatic (version 0.36) was employed to filter out low-quality reads and remove reads contaminated with adapter sequences. Clean reads were further processed using in-house scripts to address duplication bias introduced during library preparation and sequencing.

The de-duplicated sequences were aligned to the reference genome of Homo sapiens using STAR software (version 2.5.3a) with default parameters. Reads mapped to the exon regions of each gene were counted using featureCounts (Subread-1.5.1; Bioconductor), and Reads Per Kilobase per Million mapped reads values were calculated. Differential gene expression analysis between groups was conducted using the edgeR package (version 3.12.1). Statistical significance of gene expression differences was assessed using a p-value cutoff of 0.05 and a fold-change cutoff of 2. GO analysis and KEGG enrichment analysis for differentially expressed genes were performed using KOBAS software (version: 2.1.1). A p-value cutoff of 0.05 was used to determine statistically significant enrichment.

## Drug bioavailability evaluation

Solutions of seven drugs (Antipyrine, Propranolol hydrochloride, Hydrochlorothiazide, ( $\pm$ )-Sulpiride, and Ranitidine hydrochloride) were purchased from Shanghai Aladdin Biochemical Technology. Atenolol and Furosemide were purchased from Dalian Meilune Biochemical Technology. The drugs were prepared at a concentration of 2  $\mu\text{mol/ml}$  in HBSS from Meilunbio. Prior to drug absorption evaluation, cells were washed twice with HBSS for 30 minutes. Then, 150  $\mu\text{L}$  of the drug solution was added to the middle well, while 600  $\mu\text{L}$  of HBSS was added to the lower well. After a 3-hour incubation, 500  $\mu\text{L}$  of medium from the lower well was collected and centrifuged at 8000 rpm for 10 minutes. The supernatant was quantified by liquid chromatography (LC20A, Shimadzu, Japan) with a chromatographic column size of 250 mm\*4.6 mm, 5  $\mu\text{m}$ , C18. The injection volume was 10  $\mu\text{L}$ . Antipyrine was detected at a wavelength of 254 nm, Propranolol hydrochloride at 223 nm, Verapamil at 278 nm, Hydrochlorothiazide at 270 nm, Ranitidine hydrochloride at 230 nm, Atenolol at 240 nm, ( $\pm$ )-Sulpiride at 230 nm, and Furosemide at 279 nm.

## Statistical analysis

Data were expressed as the means  $\pm$  SEM and analyzed by performing Student's t-test. Significance levels were denoted as follows: \* $p < 0.05$ , \*\* $p < 0.01$ , and \*\*\* $p < 0.001$ . The sample size is at least three and all experiments have been repeated at least twice. In addition, the data were handled with Excel, PowerPoint, and GraphPad Prism.

## Result

### Design and operation of the generic organ-on-a-chip platform

As shown in **Fig. 1A**, each chip consists of 32 chip units, with each chip unit consisting of three horizontally arranged wells. The holes at both ends are connected by the passageway of the lower channel, where culture the medium was perfused with a rocker. The middle hole is designated for cell culture and is separated from the lower layer by a transparent PET porous membrane. The specifications of the porous membrane can be chosen according to specific requirements. This design not only reduces the consumption of culture medium and other materials but also facilitates pipetting operations and characterizations with enhanced convenience.

To validate the usability of the chip, we constructed a simple gut-on-a-chip model. In the specific experiments, Caco-2 and HT-29 cells were seeded in a 9:1 ratio, totaling about 50,000 cells, in the central well of the chip unit to form a compact layer of intestinal epithelial cells on the membrane (**Fig. 1B**). Then the chip was placed on a rocker at a speed of 10 rpm and an angle of  $\pm 8^\circ$  to induce basal fluid flow. To further investigate the fluid dynamics within the chip, computational simulations were performed using COMSOL software. The results indicate that the fluid shear stress ( $\sim 0.4 \text{ dyn/cm}^2$ ) at the center of the membrane was relatively lower compared to the surrounding regions ( $0.8 \sim 2 \text{ dyn/cm}^2$ ) (**Fig. 1C**). Additionally, the fluid shear stress beneath the membrane remained stable at around  $0.4 \text{ dyn/cm}^2$  (**Fig. S3**). These observed shear force values align well with physiological data.<sup>[26]</sup>

It should be noted that although we focus on seeding cells on the upper side of the membrane in this work, the chip design (**Fig. 1B**) allows for easy cell seeding on the opposite side of the membrane by simply seeding cells in the bottom channel and inverting the chip. This unique feature enables the co-culture of multiple cell types, thus highlighting the scalability of our system and its potential for diverse applications. For instance, a multicellular model of inflammatory bowel disease can be established on this platform by seeding intestinal epithelial cells in the central well, inoculating intestinal endothelial cells on the opposite side of the membrane, and introducing immune cells into the bottom channel. Additionally, the versatility of the system extends further with the ability to control the cultivation conditions. By adjusting the angle and speed of the rocker, different shear forces can be easily applied to achieve distinct cultivation conditions for various experimental needs.

### Characterization of the intestinal epithelium on the organ-on-a-chip platform

Previous studies have elucidated the crucial role of basal-side fluid flow in promoting the morphogenesis of Caco-2 cells.<sup>[27, 28]</sup> This effect is attributed to the accumulation of Wnt signaling pathway inhibitors, such as DKK-1, beneath the membrane under static conditions, leading to hindered cell proliferation and impaired morphogenesis of the Caco-2 cell layer. The introduce of fluid flow can effectively eliminate the accumulation of these inhibitory molecules. In our research, a rocker with adjustable angle and speed was employed to induce reciprocating fluid flow. This dynamic flow not only dilutes the inhibitory molecules but also facilitates the occurrence of intestinal-like morphogenesis that closely mimics *in vivo* conditions.

In our chip system, a prominent distinction was observed between the perfused and static conditions. Under perfusion conditions, the intestinal cell layer cultured on the chip developed 3D villous structures, while cells without perfusion predominantly remained in a single-layer state. After three days of culture with fluid, noticeable disparities were observed under an optical microscope (**Fig. 2A**). The intestinal cells under flow conditions formed convex and stacked structures, appearing as dark arc curves or circular structures with well-defined boundaries. Similar to transwell or petri dish culture, intestinal cells can be cultured on the chip for up to 30 days, but after the sixth day, there is no significant change in the morphology of the cells under the optical microscope (**Fig. S4**). Consequently, cells after six days of fluid introduction were taken for characterization.

Live/dead staining images revealed that most of the cells exhibited normal growth after six days of perfused culture on the chip (**Fig. 2D**). Additionally, a CCK-8 assay was performed to assess cell viability under static and perfused conditions, demonstrating that the viability of cells cultured on the chip was comparable to or even higher than that of cells cultured in a static state (**Fig. 2E**). Furthermore, differences in cell layer height and microvillus morphology were observed through H&E staining (**Fig. 2B**) and SEM (**Fig. 2C**), respectively. These results highlight the successful establishment of an intestinal-like morphogenesis on our chip system under perfusion conditions.

### Improved functionality of intestinal epithelium under flow condition

To assess the integrity of the cell layer, we evaluated the permeability of the intestinal barrier by measuring the fluorescence intensity of FITC-dextran with varying molecular weights that permeated the cell layer within a specific time frame (**Fig. 2F**). Notably, regardless of molecular weight, the  $P_{app}$  of dextran in the perfused chip was significantly lower than that observed in the static culture. In the 1-hour experiment, the  $P_{app}$  of 4 kDa-dextran was as low as  $5 \times 10^{-7}$  cm/s, indicating a substantial enhancement in the integrity of the intestinal barrier in the perfusion environment.

To further assess the integrity of the intestinal barrier, we measured the TEER using a commercially available instrument, EVOM3, which was facilitated by our chip design (**Fig. S3**). Interestingly, there was minimal disparity between the TEER values of the perfused and static cultures (**Fig. 2G**), deviating from previous studies. Both groups displayed an upward trend in TEER over the six-day culture period, eventually reaching an approximate value of  $100 \Omega \cdot \text{cm}^2$ . While this value may seem relatively low compared to other reports, it is essential to note that co-culturing Caco-2 and HT-29 cells typically leads to lower TEER values.<sup>[29, 30]</sup> Consequently, the observed TEER value aligns more closely with physiological conditions in humans.

Immunofluorescence staining of ZO-1 (**Fig. 3C**) revealed the presence of well-formed tight junctions and brush border formation in the perfusion environment, indicating a more robust barrier compared to static culture. Moreover, the detection of Villin (**Fig. 3F**) in apical cells provided additional evidence for the presence of intestinal villi in the perfusion environment, which was further supported by SEM images showing well-defined microvilli (**Fig. 2C**). Furthermore, by analyzing the distribution of nuclei in images at different levels, we could clearly visualize the hollow structure of intestinal villi (**Fig. 3A**). The expression of MUC-2 was also detected. As shown in **Fig. 3D**, MUC-2 was evenly distributed on the intestinal villus, and superposition with the bright field image provided a clear view of the villi's shape. Side-view confocal 3D images allowed us to calculate the height of the villi, and the results indicated that the average villi height in static culture was about  $33 \mu\text{m}$  (**Fig. 3E**), while the average villi height on the chip was close to  $90 \mu\text{m}$ . Additionally, the expression of Ki67 (**Fig. 3G**) indicated active proliferation of intestinal cells, suggesting

the potential for further growth into higher intestinal villi.

### Transcriptional analysis of the intestinal cells

To gain a comprehensive overview of the transcriptional responses to basal fluid, we performed RNA-seq analysis of intestinal epithelial cells in the chip. Differentially expressed genes were identified to elucidate the transcriptomic differences between the presence and absence of fluid. Based on the biological repeated correlation test of the samples, a clear distinction could be observed between the perfused and static groups, while within each group, independent reproducibility was confirmed (**Fig. 4B**). By applying the criteria of an absolute value of log fold change  $> 1$  and a p-value  $< 0.05$ , we identified 151 up-regulated genes and 304 down-regulated genes in the perfused group compared to the static condition (**Fig. 4A**).

The biological processes associated with these genes were further characterized using GO and KEGG pathway enrichment analysis. Using the GO database, we classified the differentially expressed genes into biological process, molecular function, and cell component categories. Among all the enriched terms, the biological process classification was the most prominent and of primary interest. **Fig. 4C** presents the top 20 terms in descending order of p-value. Notably, in the context of our system, several up-regulated genes of cell under fluid flow were associated with cellular activities, including “regulation of epithelial cell proliferation”, “negative regulation of endothelial cell apoptotic process”, and “cellular response to dexamethasone stimulus”. Additionally, terms related to material metabolism, such as “negative regulation of cholesterol storage”, “linoleic acid metabolic process”, and “glutathione derivative biosynthetic process”, indicated that fluid stimulation impacts the metabolic function of cells. Interestingly, in the enrichment analysis of down-regulated genes, we identified the terms “cellular response to fluid shear stress” and “cellular response to mechanical stimulus”. Furthermore, terms related to cell adhesion, such as “cell surface” and “anchored component of membrane”, were also present. Whether this is a negative feedback regulation of cells in the gut-on-a-chip system we constructed, it still needs a further exploration.

Furthermore, the KEGG enrichment analysis (**Fig. 4D**) revealed that the presence of fluid in the culture enhances several pathways associated with drug metabolism compared to static culture. These pathways include “Metabolism of xenobiotics by cytochrome P450”, “Drug metabolism - other enzymes”, and “Drug metabolism - cytochrome P450”. Moreover, the enrichment of up-regulated genes in pathways such as “Fat digestion and absorption” and “Metabolic pathways” indicates an improvement in the metabolic function of cells in the presence of fluid. These findings underscore the ability of our platform to achieve better physiological function simply by providing fluid with a rocker, as compared to regular static cultivation.

### Assessment of drug bioavailability after exposure to gut-on-a-chip

The results of RNA-seq have heightened our focus on the potential application of the gut-on-a-chip system in the field of in vitro drug bioavailability evaluation. It is well-established that various orally administered drugs exhibit different levels of absorption across the epithelial barrier in vivo. As a result, an absorption test is essential for each new drug before its clinical application. In this study, we aimed to utilize the gut-on-a-chip system to measure the permeability ( $P_{app}$ ) values of seven drugs: Antipyrine, Propranolol hydrochloride, Hydrochlorothiazide, Ranitidine hydrochloride, Atenolol, Sulpiride, and Furosemide. These drugs were selected based on the Biopharmaceutics Classification System Biowaivers Guidance for Industry, and they represent a range of high, medium, and low in vivo permeability with well-documented bioavailability.<sup>[31]</sup>

After cultivating cells on the chip using the consistent method, we employed high-performance liquid chromatography to measure the drug concentration reaching the bottom channel of the chip following a three-hour drug incubation period (**Fig. 5A**). Subsequently, we established a correlation between the drug permeability coefficient and its in-vivo bioavailability. The  $P_{app}$  values were determined using the following formula:  $P_{app} = (dQ/dt) / (A \cdot c_0)$ . In this equation,  $dQ$  represents the amount of drug passing through the membrane during the experimental duration,  $dt$  denotes the experimental time,  $A$  signifies the membrane area, and

$c_0$  corresponds to the initial concentration of the drug introduced from the apical side. The experimental results showed a clear positive correlation between the  $P_{app}$  values and bioavailability in both the static and perfused chips (**Fig. 5B**). However, the linear fit of the dynamic results was significantly superior, with an  $R^2$  value of 0.7085 for the perfused chip and only 0.3081 for the static chip. These findings indicate that the perfused chip holds greater potential as a platform for predicting drug absorption.

## Discussion

In this study, we successfully developed a generic pump-free organ-on-a-chip platform and used it to mimic the physiological characteristics of the human intestinal barrier. After determining the appropriate flow rate through fluid simulation, the intestinal cells cultured on our platform proliferate and differentiate vigorously, forming an intestinal barrier and demonstrating its function through the oscillation of the rocker to provide fluid. Subsequently, we investigated the impact of fluid dynamics on cells in our system using RNA-seq analysis, which revealed significant differences in metabolic pathways. Based on these promising results, we proceeded to evaluate the bioavailability of drugs using our gut-on-a-chip model, achieving excellent linear relationship simulations. These data conclusively confirm the applicability of our platform and its potential as a substitute for traditional organ chip models.

Looking ahead, our chip platform has the capability to simulate various human physiological systems, particularly those at the interface *in vivo*, such as the blood-brain barrier, alveoli, glomeruli, and more. By enabling the culture of different types of cells on both sides of the membrane and providing shear force through a rocker mechanism to simulate different body fluid conditions, we can further enhance the versatility of our platform. However, we recognize the need to address specific limitations and challenges to maximize the potential of our chip system. This includes enhancing the longevity and stability of cultured cells, optimizing fluidic dynamics within the chip, and expanding the range of cell types to better emulate the complexity of the human body.

In the future, we hope to establish a powerful model that integrate organ-on-a-chip technology with advanced analytical techniques and computational models aiming to transcend the limitations of animal testing, especially in drug development and toxicity studies. By leveraging these cutting-edge tools, we anticipate achieving a deeper understanding of drug behavior, leading to the identification and development of safer and more effective therapeutics, ultimately benefiting human health and transforming the landscape of pharmaceutical research.

## Acknowledgements

This research was supported by the National Key R&D Program of China (No. 2022YFA1104700), National Nature Science Foundation of China (No. 31971373, 32101163), the Strategic Priority Research Program of the Chinese Academy of Sciences, Grant (No. XDB29050301), Yunnan Key Research and Development Program (No.202003AD150009), Innovation Program of Science and Research from the DICP, CAS (DICP I202128).

## Author Contributions

Yaqiong Guo: Conceptualization, methodology, project administration, visualization, and writing-review&editing; Yingying Xie: Data curation, investigation, project administration, writing and editing. Jianhua Qin: Supervision, funding acquisition, writing-review&editing.

## Conflict of Interest

The authors declare no commercial or financial conflict of interest.

## Availability of data and materials

We declare that all data generated or analyzed during this study are included in this article.

## References

- [1] C. M. Leung, P. De Haan, K. Ronaldson-Bouchard, G.-A. Kim, *et al.*, *Nature Reviews Methods Primers* 2022, *2*, 33.
- [2] G. Vunjak-Novakovic, K. Ronaldson-Bouchard, M. Radisic, *Cell* 2021, *184*, 4597-4611.
- [3] D. E. Ingber, *Nat. Rev. Genet.* 2022, *23*, 467-491.
- [4] C. Xian, J. Zhang, S. Zhao, X. G. Li, *J Tissue Eng* 2023, *14*, 20417314221149882.
- [5] D. Marrero, F. Pujol-Vila, D. Vera, G. Gabriel, *et al.*, *Biosens Bioelectron* 2021, *181*, 113156.
- [6] R. Novak, M. Ingram, S. Marquez, D. Das, *et al.*, *Nature biomedical engineering* 2020, *4*, 407-420.
- [7] O. Y. F. Henry, R. Villenave, M. J. Crouce, W. D. Leineweber, *et al.*, *Lab on a Chip* 2017, *17*, 2264-2271.
- [8] B. Srinivasan, A. R. Kolli, M. B. Esch, H. E. Abaci, *et al.*, *J Lab Autom* 2015, *20*, 107-126.
- [9] H. J. Chen, P. Miller, M. L. Shuler, *Lab Chip* 2018, *18*, 2036-2046.
- [10] S. J. Trietsch, E. Naumovska, D. Kurek, M. C. Setyawati, *et al.*, *Nat. Commun.* 2017, *8*, 262.
- [11] H. B. Chong, J. Youn, W. Shin, H. J. Kim, D. S. Kim, *Lab Chip* 2021, *21*, 3316-3327.
- [12] Y. Wang, Z. Shao, W. Zheng, Y. Xie, *et al.*, *Biofabrication* 2019, *11*, 045001.
- [13] J. Deng, W. Wei, Z. Chen, B. Lin, *et al.*, *Micromachines* 2019, *10*, 676.
- [14] R. R. Xiao, B. Jing, L. Yan, J. Li, *et al.*, *Lab Chip* 2022, *22*, 4481-4492.
- [15] H. J. Kim, D. Huh, G. Hamilton, D. E. Ingber, *Lab on a Chip* 2012, *12*, 2165-2174.
- [16] Y. Guo, R. Luo, Y. Wang, P. Deng, *et al.*, *Sci Bull (Beijing)* 2021, *66*, 783-793.
- [17] Q. Ramadan, H. Jafarpoorchekab, C. Huang, P. Silacci, *et al.*, *Lab Chip* 2013, *13*, 196-203.
- [18] H. J. Kim, H. Li, J. J. Collins, D. E. Ingber, *Proc Natl Acad Sci U S A* 2016, *113*, E7-15.
- [19] M. Maurer, M. S. Gresnigt, A. Last, T. Wollny, *et al.*, *Biomaterials* 2019, *220*, 119396.
- [20] M. S. Jeon, Y. Y. Choi, S. J. Mo, J. H. Ha, *et al.*, *Nano Converg* 2022, *9*, 8.
- [21] W. Shin, H. J. Kim, *Proc Natl Acad Sci U S A* 2018, *115*, E10539-E10547.
- [22] P. A. Billat, E. Roger, S. Faure, F. Lagarce, *Drug Discov Today* 2017, *22*, 761-775.
- [23] S. Youhanna, V. M. Lauschke, *J Pharm Sci* 2021, *110*, 50-65.
- [24] J. P. Gleeson, F. McCartney, *Trends Pharmacol Sci* 2019, *40*, 720-724.
- [25] C. Ma, Y. Peng, H. Li, W. Chen, *Trends Pharmacol. Sci.* 2021, *42*, 119-133.
- [26] C. Dewey Jr, S. Bussolari, M. Gimbrone Jr, P. F. Davies, 1981.
- [27] W. Shin, C. D. Hinojosa, D. E. Ingber, H. J. Kim, *iScience* 2019, *15*, 391-406.
- [28] W. Shin, H. J. Kim, *Nat Protoc* 2022, *17*, 910-939.
- [29] N. Ashammakhi, R. Nasiri, N. R. Barros, P. Tebon, *et al.*, *Biomaterials* 2020, *255*, 120196.
- [30] A. Beduneau, C. Tempesta, S. Fimbel, Y. Pellequer, *et al.*, *Eur J Pharm Biopharm* 2014, *87*, 290-298.
- [31] H. Chavda, C. Patel, I. Anand, *Systematic reviews in pharmacy* 2010, *1*, 62.

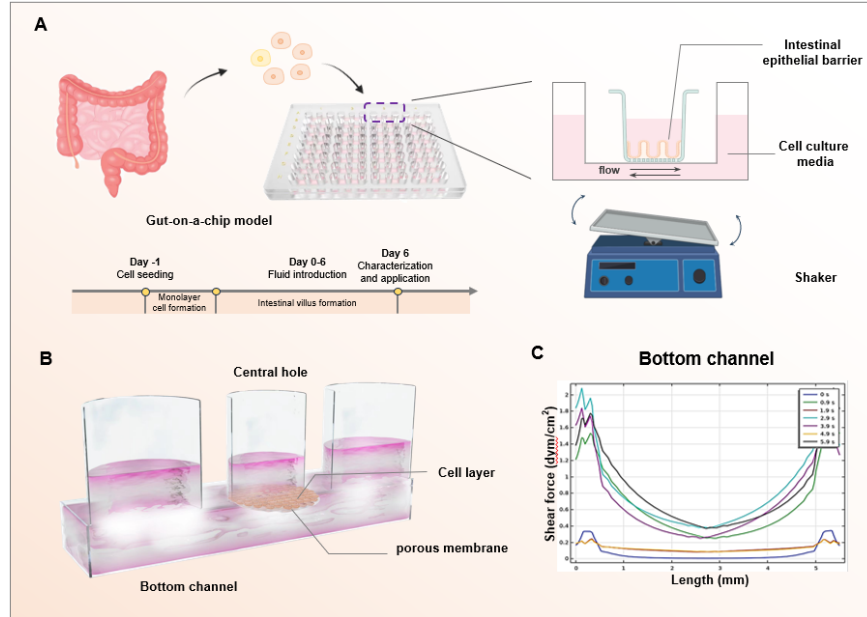


**Fig 1. Schematic illustration of the platform.** (A) The schematic of chip and cell culture. The chips are transferred onto a rocker placed in a cell culture incubator 24 hours after cell seeding. (B) 3D sectional view of the chip. The central hole displays the cell culture in the upper layer and the fluid flow in the interconnected lower layer. (C) Computational simulations reveal the magnitude of fluid shear stress above the membrane.

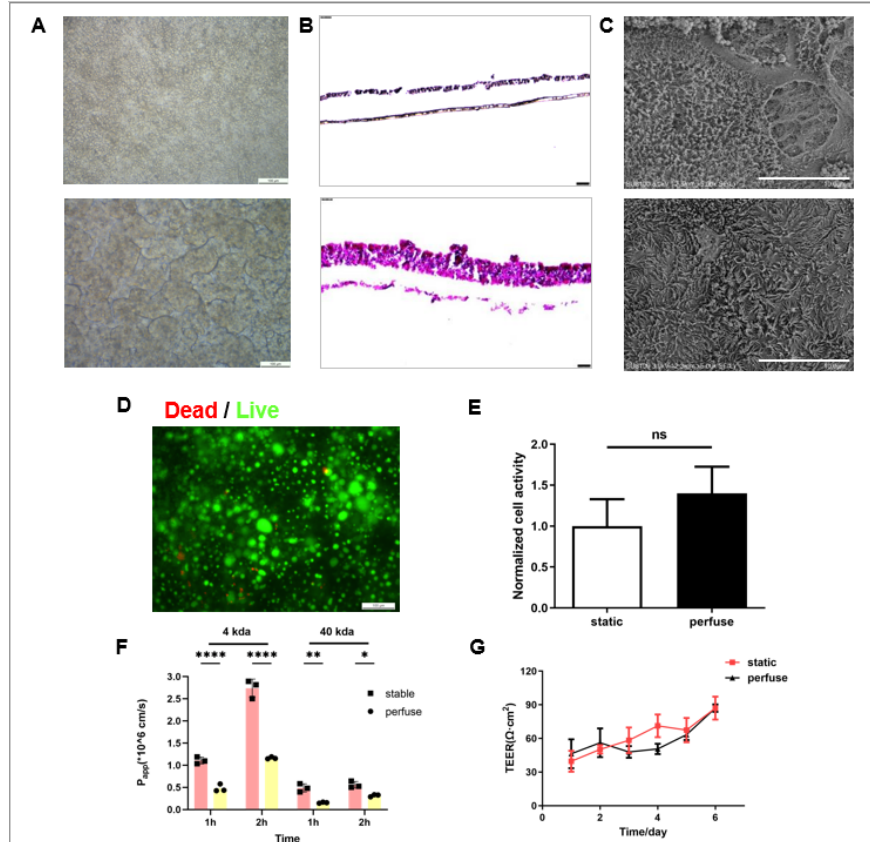


**Fig 2. Characterization of the intestinal epithelium on the organ-on-a-chip platform.** (A) Microscopic bright field image (Scale bar: 100 um), (B) side HE staining image (Scale bar: 100 um) and (C) SEM image (Scale bar: 10 um) of chip without (up) /with (down) fluidic force provided by rocker. (D) Live/Dead staining in static chip and perfused chip (Scale bar: 100 um). (E) Cell activity in static chip and perfused chip by CCK-8 kit. (F) Permeability test by detecting the fluorescence intensity of FITC-Dextran crossing through the cell layer within a certain time. (G) The TEER value of static chip (red) and perfused chip (black).

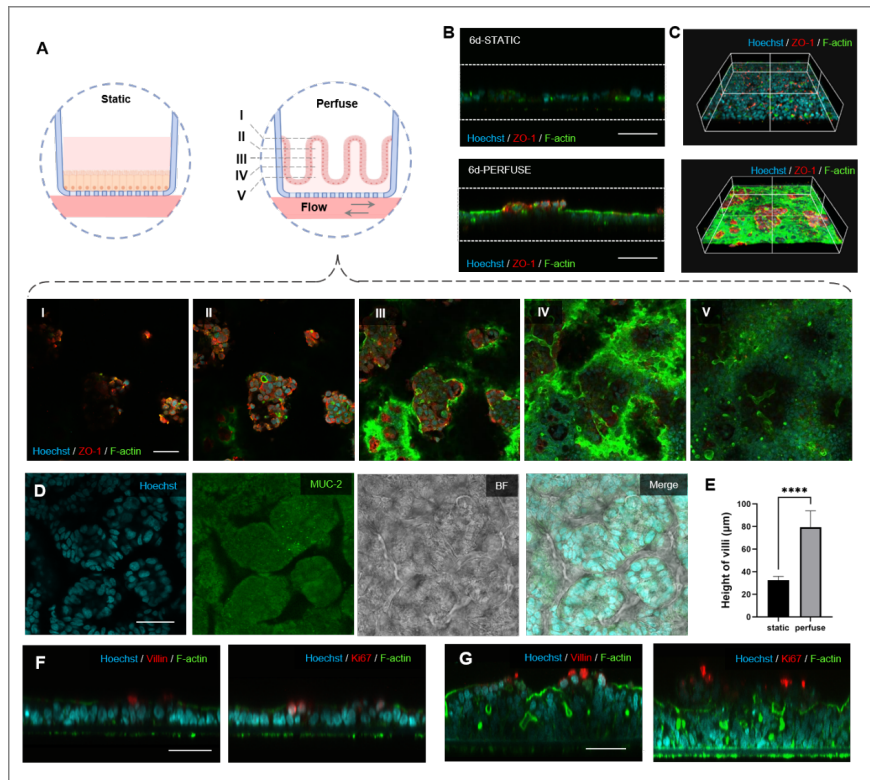


**Fig 3. Morphologic and differential characterization of the intestinal epithelium on the gut-on-a-chip platform.** (A) The longitudinal section of chip and the immunofluorescence images of cells cultured in gut-on-a-chip with fluidic force, in which expression of ZO-1 (red) at different height could be observed. Corresponding to the schematic, I represents apical side and sequentially V represents basal side. Besides, nuclei are dyed by Hoechst (blue) while F-actin is marked by phalloidin (green), the same below. (Scale bar: 50 µm). (B) Cross-sectional view of expression of ZO-1 in static chip (top) and perfused chip (below). (Scale bar: 100 µm). (C) The integral 3D image of intestinal cells layer in static chip (top) and perfused chip (below). (D) Expression of MUC-2 in perfused chip (Scale bar: 50 µm). (E) The height of villi measured by Image J according to the side view of immunofluorescence. (F&G) Cross-sectional view of expression of Villin and Ki67 in static chip (F) and perfused chip (G) (Scale bar: 50 µm).

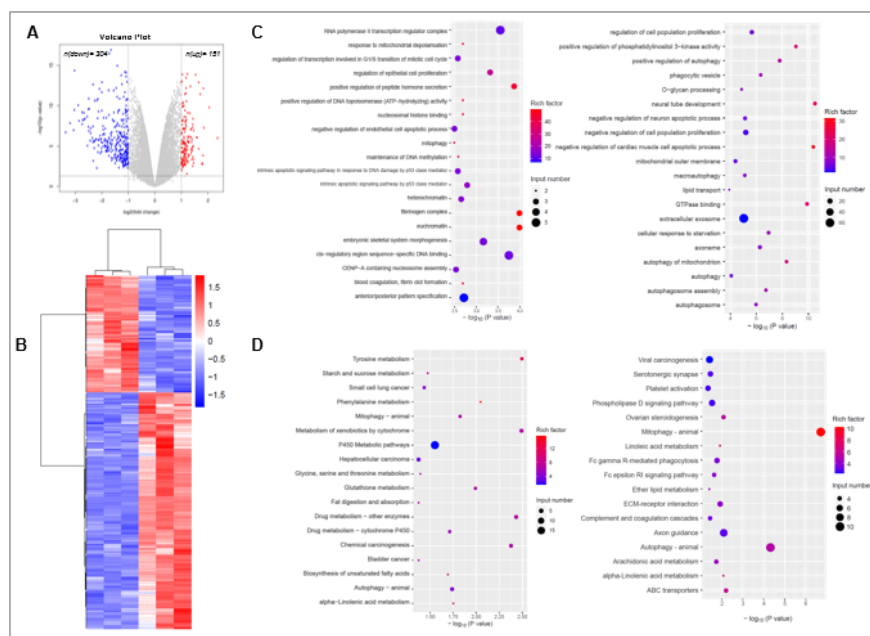


**Fig 4. Transcriptional analysis of the cells in perfused or static condition.** (A) Volcano plots of the dysregulated genes in perfusion culture. (B) Cluster analysis of differentially expressed genes. (C) GO and (D) KEGG pathway enrichment analysis of perfused chip contrast static chip up-regulation (left) /down-regulation (right) differentially expressed genes.

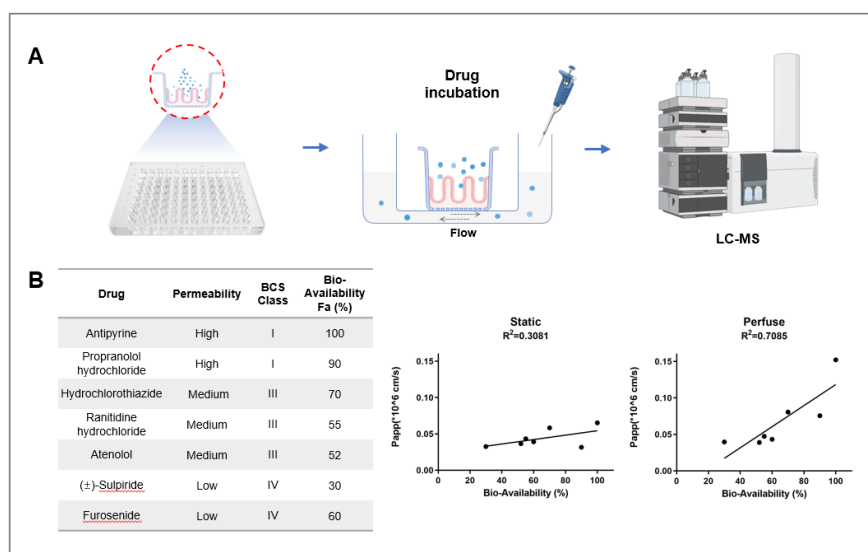


**Fig 5. Application of gut-on-a-chip in drug bioavailability assessment.** (A) The schematic of high throughput gut-on-a-chip used in drug absorption prediction experiment. (B) Comparison of drug permeation across cell barrier formed on static or perfused chip with human in vivo bio-availability. Every point in the plot represents a drug in the table.